Green One-pot Synthesis of a Curcumin Nanomedicine through Bioinspired Polymerization of Quercetin: In Vitro and Preliminary In Vivo Evaluation

Suhair Sunoqrot[a]*, Tahany Al-Debsi[a], Eveen Al-Shalabi[a], Lina Hasan[a], Farid Mohammad Faruqu[b], Adam Walters[b], Khuloud T. Al-Jamal[b], and Robert Palgrave[c].

[a]*Department of Pharmacy, Faculty of Pharmacy, Al-Zaytoonah University of Jordan, Amman 11733, Jordan*

[b]*Institute for Pharmaceutical Science, King's College London, London SE1 9NH, UK*

[c]*Department of Chemistry, University College London, London WC1H 0AJ, UK*

*Corresponding Author:

Suhair Sunoqrot, PhD

Assistant Professor of Pharmaceutics

Department of Pharmacy

Faculty of Pharmacy

Al-Zaytoonah University of Jordan

P.O. Box 130, Amman 11733, Jordan

Phone: +962-6-4291511 Ext. 312

Fax: +962-6-4291432

Email: suhair.sunoqrot@zuj.edu.jo

Abstract

Nanomedicine has had a profound impact on the treatment of many diseases especially cancer. However, synthesis of multifunctional nanoscale drug carriers often requires multistep coupling and purification reactions, which can pose major scale-up challenges. Here we leveraged oxidation-triggered polymerization of catechols to synthesize nanoparticles (NPs) from the plant polyphenol quercetin (QCT) loaded with a hydrophobic anti-cancer drug, curcumin, and functionalized with poly(ethylene glycol) (PEG) for steric stabilization in one reaction step. NPs were formed by base-catalyzed oxidative self-polymerization of QCT in the presence of curcumin and thiol-terminated PEG in DMSO, followed by self-assembly upon the gradual addition of water. Surface modification of the NPs with PEG was confirmed by dynamic light scattering and X-ray photoelectron spectroscopy. Drug loading was verified by UV-Vis spectroscopy. Curcumin-loaded NPs were readily internalized by CT26 murine colon cancer cells as determined by flow cytometry and confocal microscopy. NPs also demonstrated sustained drug release and potent cytotoxicity in vitro. Moreover, in vivo imaging of CT26 tumor-bearing Balb/c mice following tail vein injection of DiR-labeled NPs showed steady tumor accumulation of the NPs up to 24 h. This was further supported by significant tumor uptake of curcumin-loaded NPs as measured by flow cytometry analysis of tumor homogenates. Our findings present a promising green anti-cancer nanomedicine that can be synthesized from renewable sources at low cost with minimal equipment.

Keywords: Quercetin; curcumin; nanoparticles; cancer targeting; green chemistry

Cancer is the leading cause of death globally, responsible for 9.6 million deaths in 2018.[1] Nonspecific uptake of small molecule anti-cancer drugs, which often results in severe side effects, can be effectively mitigated by nanoscale drug carriers.[2-4] Among the various types of nanocarriers available, a common denominator is the fact that the nanocarrier surface needs to be modified in order to impart functionalities such as prolonged in vivo half-life, reduced immunogenicity, and selective cellular targeting.[5-6] Surface modification techniques typically involve chemical conjugation of the desired ligand to the nanocarrier individual components before formation,[7-8] or conjugation to preformed nanocarriers using reactive linkers or coupling agents.[9-10] These techniques may also require exhaustive purification processes, which can be lengthy and inefficient and must be tailored for each ligand. The additional synthetic steps required can also lead to increased costs and greater regulatory hurdles.

Naturally-occurring polyphenols have attracted considerable attention in the past decade due to their unique features as biocompatible coating precursors for two- as well as three-dimensional surfaces.[11] Polyphenols such as dopamine, pyrogallol, tannic acid, and catechins undergo oxidation-triggered self-polymerization in aqueous alkaline buffers, forming stable surface coatings onto a wide range of substrates. For example, Lee et al. used dopamine self-polymerization to form thin, surface-adherent polydopamine films onto a wide range of organic and inorganic materials, such as polymers, metals, semiconductors, and ceramics.[12-13] Li et al. synthesized polyphenol-coated mesoporous silica nanoparticles, which improved colloidal stability, prevented premature drug leakage, and also provided a scaffold for immobilization of targeting moieties such as aptamers.[14] In another example, Sileika et al. developed a generally applicable process for the surface modification of solid, porous nanoparticulate metal, ceramic, and polymer materials based on the observation that polyphenol compounds found in tea, red

wine and chocolate may form thin adherent films on various substrates by spontaneous adsorption from solution.(Sileika et al. 2013) Abouelmagd et al. reported tannic acid (TA) as a coating precursor that is comparable to polydopamine. TA formed a stable and optically inert coating on polymeric NPs, enabling the surface incorporation of albumin, chitosan, and folate-terminated PEG [15].

The oxidized catechol moieties in these coatings have been shown to mediate ligand incorporation through covalent bonding with amine- and thiol-bearing ligands, hydrogen bonding, π-π stacking, and metal coordination.[16] These features have inspired the development of standalone NPs as potential drug delivery nanocarriers, with the additional advantage of facile surface modification with desired ligands by relying on the reactivity of the oxidized catechols without using complex coupling reagents, unlike existing NP therapeutics. Such polyphenol NPs have been reported using dopamine[17-18] and green tea polyphenols.[19-21]

We have recently devised a simple NP synthesis technique by relying on the biologically-inspired phenomenon of oxidation-triggered polymerization of plant polyphenols.[22] Using quercetin (QCT) as the NP precursor, we observed that it could undergo oxidative self-polymerization simply by mixing in an aqueous alkaline buffer, forming spherical NPs 30-40 nm in diameter. The NPs were sequentially functionalized with amine-terminated poly(ethylene glycol) (PEG) as an anti-fouling polymer and a model surface ligand, and a small molecule anti-cancer drug, doxorubicin (DOX). PEGylation and drug loading were facilitated by the reactivity of oxidized catechol moieties toward nucleophiles, and the ability to form H-bonding and π-π stacking interactions with like molecules. Drug-loaded NPs showed high loading capacities, sustained release, and potent cytotoxicity in vitro.

Our QCT-based multifunctional NP platform was synthesized at ambient conditions without the use of any coupling reagents, and the purification process only involved ultrafiltration. However, the first-generation NPs were synthesized under aqueous conditions, which only allowed the incorporation of water-soluble drugs such as DOX. In addition, NP synthesis, surface functionalization, and drug loading were performed in sequential steps over several days, which may be inefficient for future scale-up efforts. For these reasons, we set out to harness the polymerization potential of natural polyphenolic compounds such as QCT to synthesize functionalized NPs via a new one-pot procedure that would allow polyphenol polymerization and simultaneous incorporation of surface ligands and poorly water soluble cargo. We hypothesized that oxidative self-polymerization of QCT can be triggered in an organic solvent such as dimethylsulfoxide (DMSO) by the presence of a strong base, rendering the oxidized catechol moieties of QCT reactive toward a nucleophilic ligand such as thiol-terminated PEG. The synthesized "amphiphile" of PEG-QCT oligomers would then form colloidal assemblies upon the addition of water. We further hypothesized that by adding a hydrophobic drug to the reaction mixture in DMSO, the former would become entrapped in the NP core during self-assembly, forming a PEGylated drug-loaded nanocarrier. Curcumin (CUR) was chosen as a model hydrophobic cargo for its reported anti-cancer activity, its polyphenolic structure which would facilitate loading into QCT NPs, and its fluorescent nature that would facilitates NP tracking in vitro and in vivo.

NPs were characterized by dynamic light scattering (DLS) and scanning electron microscopy (SEM) to verify their size and morphology. Surface PEGylation was confirmed by surface charge measurements, X-ray photoelectron spectroscopy (XPS), and Fourier transform-infrared (FT-IR) spectroscopy. CUR loading and release, cellular uptake, and cytotoxicity

experiments in CT26 murine colon cancer cells supported the viability of the one-pot method to produce functional CUR-loaded NPs with potent anti-cancer activity. Finally, passive targeting of the NPs to CT26 tumors was investigated by in vivo imaging and flow cytometry, further validating the potential of the newly designed green NPs as an anti-cancer nanomedicine.

Results

Synthesis and characterization of CUR-loaded PEGylated QCT NPs

An overview of the one-pot NP synthesis procedure is outlined in Figure 1A, and a proposed mechanism for QCT NP formation is shown in Figure 1B. We have previously shown that QCT undergoes oxidative coupling in basic aqueous conditions yielding oligomers of ~5 monomers that are further stabilized by noncovalent interactions forming spherical colloidal aggregates.[22] In this study, TEA was used to catalyze QCT polymerization in DMSO, and NP formation was induced by solvent exchange in a process similar to self-assembly of amphiphilic copolymers during micelle formation.

As shown in Table 2, QCT alone (C1) formed NPs around 33.4 nm in size, similar to our previous findings.[22] The FT-IR spectrum of QCT (Figure S1) exhibited the characteristic bands corresponding to O-H stretching (3416 and 3330 cm^{-1}), C=O stretching (1668 cm^{-1}), C=C aromatic stretching (1612, 1562, and 1522 cm^{-1}), and O-H bending (1382 cm^{-1}). The spectrum of QCT NPs (C1) showed similar peaks, indicating that no new functional groups were formed after oxidation and polymerization. The UV-Vis spectra of QCT and QCT NPs (C1) in methanol before and after the addition of NaOMe, $AlCl_3$, and $AlCl_3$/HCl were used to determine the oxidation state of QCT before and after polymerization.[23-25] As depicted in Figure S2, QCT showed absorption bands at 256 nm (band II) and 371 nm (band I). A bathochromic shift to 422 nm for band I was observed after adding NaOMe, which confirms the presence of a free -OH group at C-3. In addition, the appearance of a new peak at 327 nm indicates the presence of a free -OH group at C-7. A bathochromic shift to 428 for band I upon the addition of $AlCl_3$/HCl confirmed the presence of free -OH groups on C-3 and C-5. A bathochromic shift to 457 nm for band I was observed upon the addition of $AlCl_3$, which was greater than that in $AlCl_3$/HCl by 29

nm, indicating the presence of *o*-dihydroxyl groups on ring B. On the other hand, the UV-Vis spectrum of QCT NPs (C1) showed absorption bands at 257 nm for band II and 348 nm for band I. A 128 nm bathochromic shift to 476 nm for band I was observed after the addition of NaOMe, confirming the presence of a free -OH group at C-3. The appearance of a new peak at 390 nm indicates the presence of a free -OH group at C-7. A bathochromic shift of 97 nm to 445 nm for band I was observed after adding $AlCl_3$, but was not affected by the addition of HCl. This confirms the presence of free -OH groups on C-3 and C-5, and the absence of *o*-dihydroxyl groups on ring B, which signifies that the catechol groups on ring B have been oxidized to quinones, making them unavailable for complexation with $AlCl_3$ (Figure S2).

PEGylated NPs were obtained by adding mPEG-SH to the reaction in DMSO by exploiting the fact that the oxidized catechols on ring B of QCT are susceptible to nucleophilic addition reactions (Figure 1B), facilitating the incorporation of amine- or thiol-terminated ligands. Upon incorporation of mPEG-SH, NP size was increased to 165.6 nm (C2). This is consistent with previous reports, where surface PEGylation of polyphenol NPs led to an increase in the hydrodynamic diameter depending on the conformation of the PEG chains.[18, 26] Additionally, the FT-IR spectrum of PEGylated QCT NPs (C2) (Figure S1) exhibited C-H and C-O-C stretching bands at 2891 cm^{-1} and 1110 cm^{-1}, respectively, corresponding to the presence of PEG.

A DPPH assay was conducted comparing the scavenging activity of QCT NPs (C1) to unmodified QCT (Figure S3). QCT is a potent antioxidant, with 25 μg causing 84.1% reduction in the formation of DPPH radicals, and 94.6% quenching at 125 μg. QCT NPs exhibited a decrease in their antioxidant activity, with 20.7% scavenging activity observed at 25 μg and

78.3% at 125 µg. Nonetheless, antioxidant activity of QCT NPs was not completely diminished, indicating that some phenolic groups were still in their reduced form even after NP formation.

The ability of the NPs to incorporate CUR with or without surface PEGylation was investigated by adding CUR at different molar ratios relative to QCT. As depicted in Table 2, NPs prepared at QCT: CUR ratios of 1:1, 1:0.5, and 1:0.1 (NP1, NP2, and NP4, respectively) were in the size range 76.4 – 96.6 nm and had polydispersity indices (PDI) ranging from 0.22 – 0.38. Drug loading efficiency was lowest for NP1 and NP2 (4.7 and 9.9%, respectively). NP3 with a QCT: CUR ratio of 1:0.25 exhibited the smallest PDI (0.05), and the highest loading efficiency (91.0%), indicating that an optimum loading capacity was reached. The significant size increase observed in NP3 (139.9 nm) was likely attributed to the greater amount of CUR incorporated compared to the other formulations. Having obtained NPs with the narrowest size distribution and the highest loading capacity with NP3, a QCT: CUR ratio of 1:0.25 was chosen for the synthesis of PEGylated CUR-loaded NPs (NP5). The NPs exhibited a spherical morphology (Figure 2A), a mean hydrodynamic diameter of 90.2 nm, a relatively narrow size distribution with a PDI of 0.12, and a loading efficiency of 51.1% (Table 2). The smaller particle size of NP5 compared to its nonPEGylated counterpart correlates with the slightly reduced drug loading capacity and may indicate possible steric hindrance imparted by the PEG chains. CUR loading did not result in any spectral changes as observed by UV-Vis (Figure S4), which signifies that CUR is only physically entrapped within the NPs.

Zeta potential measurements were conducted in order to confirm successful incorporation of PEG on the NP surface, as PEG is a neutral polymer whereas QCT carries a partially negative surface charge due to the presence of electron-rich aromatic rings. As observed in Table 2, all NPs displayed negative zeta potential values ranging from -11.3 to -21.7 mV, as previously

reported for QCT NPs.[22] However, the PEGylated formulations, C2 and NP3, displayed significantly lower surface charge values ($p < 0.001$ and $p < 0.0001$ for C2 and NP5, respectively) compared to their nonPEGylated counterparts, C1 and NP3 (Figure 3A). These findings strongly indicate partial shielding of the negative surface charge of QCT by the PEG corona.

NP PEGylation was further verified by XPS to obtain the surface elemental composition of the synthesized NPs. PEGylated NPs (C2 and NP5) showed a significant increase in S 2p signals at a binding energy of ~163 eV attributed to the presence of thiol groups of mPEG-SH (Figure 3C). Moreover, PEGylated NPs were associated with a significantly lower C/O ratio (Figure 3D) and an increase in C-O-C components (Figure S5 and Figure S6), consistent with XPS measurements of PEGylated NPs.[15, 18, 22] These findings combined with surface charge measurements corroborate our hypothesis that the one-pot procedure can successfully yield surface-functionalized QCT NPs.

In vitro release of CUR from CUR-loaded NPs

CUR release from NP5 was investigated in PBS at pH 7.4 up to 4 days. As shown in Figure 4, drug release was sustained over the period of the study, with 50.9% of the loaded amount released within the first 4 h, 95.0% released after 24 h, and 99.1% released after 4 days. Interestingly, we observed slower release with the prototype QCT NPs encapsulating DOX, where only 47.1% of DOX was released within 24 h and 70.7% released after 4 days.[22] The marked difference in release kinetics suggest a weaker interaction between CUR and QCT compared to DOX, which facilitated drug release.

Cytotoxicity of CUR-loaded NPs in CT26 cells

Cytotoxicity assays were conducted in order to verify whether the NP synthesis method compromised CUR's pharmacologic activity. CT26 cells were incubated with increasing concentrations of CUR alone or loaded in QCT NPs (NP3 and NP5) up to 72 h to allow sufficient time for CUR to be internalized and exert its effect. Another set of cells was treated with drug-free NPs (C2), which were found to be nontoxic up to 1 mg/mL (Figure S7). As shown in Figure 5, CUR exhibited dose-dependent cytotoxicity with an IC50 of 28.5 μM, which was similar to values reported in the literature.[27] PEGylated CUR-loaded NPs (NP5) showed similar potency with an IC50 of 34.7 μM. On the other hand, a marked reduction in potency was observed with nonPEGylated NPs (NP3), with an IC50 of 128.3 μM. The difference may be attributed to the greater steric stability of NP5 in the cell culture medium imparted by the surface-exposed PEG chains. The nonPEGylated NPs were more prone to aggregation, which likely hindered their cellular uptake. Although the new NP formulation of CUR did not significantly enhance its cytotoxicity, the NPs were completely soluble in water unlike free CUR.

Cellular uptake of CUR-loaded NPs by confocal microscopy and flow cytometry

Intracellular uptake of CUR alone or loaded in QCT NPs (NP3 and NP5) was visualized by confocal microscopy, enabled by the intrinsic fluorescence of CUR. CT26 cells were treated with 20 μM of CUR or an equivalent concentration in QCT NPs for 24 h. As observed in Figure 6A, stronger green fluorescence signals were obtained from CUR- and NP5-treated cells compared to NP3-treated cells. The results were consistent with the cytotoxicity experiments, were NP3 exhibited the lowest potency compared to NP5 and the free drug, which further

confirms reduced cellular uptake of the nonPEGylated NPs due to their lower stability in the culture medium. Cellular internalization was also measured by flow cytometry, by quantifying cell-associated mean fluorescence intensities (MFI) (Figure 6B and Figure 6C). CUR and NP5 showed similar MFI values, which were both significantly higher than those associated with NP3, in line with confocal microscopy observations. Taken together, the cytotoxicity and cellular uptake experiments provided strong evidence on the successful synthesis of functional NPs that are readily internalized by the cells with demonstrated in vitro anti-cancer activity.

In vivo biodistribution and tumor uptake of systemically-administered NPs

Having shown promising bioactivity in vitro, in vivo biodistribution studies were carried out on PEGylated NPs in CT26 tumor-bearing mice. NPs were loaded with DiR to enable whole body imaging over the time course of the study (24 h), and ex vivo imaging of excised major organs afterwards. Representative dorsal view images of control and NP-treated animals are shown in Figure 7A, while images of excised organs and their corresponding fluorescence intensities (expressed as total radiant efficiency per g organ) are depicted in Figure 7B and Figure 7C, respectively. Tumor accumulation of DiR-labeled NPs can be clearly observed over the time course of the study, as indicated by the steady increase in fluorescence signal intensities at the tumor sites from 1 h to 24 h. Excised tumors showed significantly lower fluorescence intensities than the spleen and lung ($p < 0.0001$) (Figure 7C), which may indicate that the NPs were mainly accumulated in the vasculature surrounding the tumors at 24 h post-injection. For this reason, tumor excision for CUR NP-treated animals was performed at 30 h post-injection, to enable more tumor uptake to take place. Flow cytometry analysis of tumor homogenates after the administration of NP5 at a dose of 6 mg/kg CUR showed significantly higher MFI compared to

PBS-treated controls (Figure 8), indicating tumor uptake of the NPs following systemic administration.

Discussion

Oxidative self-polymerization of polyphenols has attracted a great deal of attention over the past decade, and has mainly been applied to produce versatile multifunctional coatings on a variety of substrates.[11, 28] It has also inspired the development of standalone NPs from coating precursors such as dopamine, tannic acid, green tea polyphenols, and most recently, QCT. Polyphenol NPs have been synthesized through a variety of approaches, all of which have relied on oxidation-triggered polymerization of the polyphenol precursor. This may be achieved in aqueous alkaline solutions[17-18, 22, 26, 29-30] or using an oxidizing agent such as hydrogen peroxide,[31] sodium metaperiodate,[32] or copper sulfate.[19, 21], with or without the aid of a chelating agent such as ferric chloride.[33] The reactive nature of these NPs was exploited to functionalize them with surface ligands, drugs, or imaging agents through sequential incubation with the molecule of interest, followed by additional purification steps. We present in this work a straightforward greener approach to polyphenol NP synthesis where NP formation, hydrophobic drug loading, and surface functionalization can be achieved in one step. The new procedure was carried out at ambient conditions and cut down on reaction time and energy consumption.

UV-Vis analysis revealed that the catechol groups of the second generation QCT NPs were oxidized to quinones, similar to what we observed in the prototype NPs, suggesting that they were formed via a similar mechanism, i.e. oxidative self-polymerization (Figure 1B). TEA triggered the deprotonation/oxidation of the catechol moieties in QCT to form reactive quinones, which was likely followed by a cascade of C-C and C-O coupling reactions that resulted in the formation of QCT oligomers. Solvent exchange with water via dialysis allowed these oligomers to self-assemble into nanoscale spherical aggregates stabilized by non-covalent interactions. Polyphenol polymerization in nonaqueous media has only been reported for dopamine, where various substrates

were coated with polydopamine in organic protic solvents (ethanol or methanol) containing piperidine to deprotonate the catechol moieties and various ligands for simultaneous functionalization.[34] In the current work, we demonstrate that polyphenol polymerization can also be achieved in DMSO, an aprotic universal solvent, which holds great promise for translating the procedure to water insoluble polyphenol NP precursors and cargo.

Although it was decreased, QCT NPs still maintained significant free-radical scavenging activity, which is in line with previous findings that not all catechol moieties are consumed during oxidative coupling of polyphenols to form NPs.[17, 22, 26] When we tested the ability of the NPs to incorporate CUR, an optimum drug loading capacity and NP polydispersity were achieved at a QCT: CUR molar ratio of 1:0.25, which produced the largest size NPs. Interestingly, when the same QCT: CUR ratio was used to synthesize PEGylated NPs, it resulted in a decrease in the hydrodynamic diameter and a lower drug loading capacity. These observations may be attributed to steric hindrance imparted by the PEG chains, which possibly interfered with CUR loading, resulting in smaller size NPs.

We investigated the viability of the one-pot procedure to produce surface-functionalized NPs by FT-IR, DLS, and XPS measurements, all of which verified the presence of surface-immobilized PEG. PEGylation was also confirmed indirectly by observing enhanced cellular uptake and cytotoxicity of PEGylated CUR-loaded NPs (NP5) compared to nonPEGylated NPs (NP3), which was likely due to the steric stability imparted by the PEG corona in serum-containing media.

In vitro release of CUR was conducted under physiologically relevant conditions, achieving sustained release of the drug over several days. CUR released from the NPs maintained its bioactivity, which was demonstrated by the comparable potency between NP5 and

free CUR against CT26 cells. The NPs were readily internalized by the cells within 24 h as confirmed by confocal microscopy and flow cytometry. The promising in vitro performance of the NPs led us to investigate their biodistribution in vivo. PEGylated DiR-labeled QCT NPs were injected into CT26 tumor-bearing mice, and in vivo imaging up to 24 h revealed their gradual tumor accumulation. Ex vivo imaging of excised tumors showed significantly higher NP accumulation in the spleen and lung compared to the tumors. The discrepancy between in vivo and ex vivo imaging results may be attributed to the accumulation of the NPs in the tumor vasculature, and that more time was needed for tumor uptake. Thus, when tumor-bearing animals were injected with CUR-loaded NPs up to 30 h, measurable amounts of CUR were detected by flow cytometry analysis of excised tumor homogenates. Given the heterogeneous nature of tumor tissues and the less reliable EPR effect, it is evident that the synthesized NPs would greatly benefit from an active targeting mechanism. The versatile nature of QCT NPs is expected to allow the convenient fabrication of active targeted NPs to achieve more selective tumor accumulation and minimize off-target uptake. Taken together, these preliminary findings revealed valuable information about the in vivo fate of QCT NPs as a promising cancer-targeted delivery platform.

Conclusion

In this work, we tested the hypothesis that a functional anti-cancer nanomedicine can be synthesized from the abundant plant polyphenol QCT in a green one-pot procedure. PEGylated CUR-loaded QCT NPs were synthesized by base-catalyzed oxidative self-polymerization of QCT in an organic solvent, making the oxidized catechol moieties of QCT reactive toward a nucleophilic ligand such as thiol-terminated PEG. The NPs were formed upon gradual addition of water, entrapping CUR in the core. Characterization of the NPs by various techniques confirmed our hypothesis. Bioassays in a murine colon cancer model revealed the potent cytotoxicity and efficient cellular uptake of CUR-loaded NPs. In vivo biodistribution studies demonstrated the NPs' passive targeting potential and shed important insights into their in vivo fate. The unique features of these NPs make them promising candidates as versatile nanocarriers with the ability to incorporate hydrophobic drug molecules and surface ligands in a simple procedure with minimal equipment.

Experimental

Materials

Quercetin hydrate (> 95%) (QCT) was obtained from Acros Organics (Geel, Belgium), curcumin (CUR), 2,2-diphenyl-1-picrylhydrazyl (DPPH), aluminum chloride ($AlCl_3$), hydrochloric acid (HCl, 10 N), and sodium methoxide (NaOMe) were obtained from Sigma-Aldrich (St. Louis, MO, USA), 1,1'-dioctadecyl-3,3,3',3'-tetramethylindotricarbocyanine iodide (DiR) was obtained from Invitrogen (Thermo Fisher Scientific, Waltham, MA, USA), dimethyl sulfoxide (DMSO), triethylamine (TEA), and Tween 20 were obtained from Tedia (Fairfield, OH, USA), methoxy poly(ethylene glycol)-thiol, MW 5000 (mPEG-SH) was obtained from Laysan Bio (Arab, AL, USA), phosphate buffered saline 10X (PBS) was obtained from Biowest (Nuaillé, France), Ultrapure (Type 1) water (specific resistivity ~18.2 MΩ.cm at 25 °C) was prepared using a Direct-Q 5UV water purification system (EMD Millipore, Billerica, MA, USA).

Preparation of CUR-loaded QCT NPs

CUR-loaded QCT NPs were synthesized by base-catalyzed oxidative self-polymerization of QCT as previously described with some modification.[22] In a typical procedure, QCT (10 mg, 0.033 mmol) was mixed with TEA (9.2 μL, 0.066 mmol) and different amounts of CUR in 1 mL DMSO. The solution was vigorously stirred at room temperature overnight protected from light. The next day, ultrapure water (3 mL) was added dropwise under vigorous mixing for 1 h to induce NP self-assembly. After which the NPs were transferred to a dialysis membrane with 12 – 14 kD MWCO (Spectra/Por 2, Spectrum Laboratories Inc., Rancho Dominguez, CA, USA) and dialyzed against RO filtered water for two days to remove unreacted species and unentrapped

drug. NPs were later centrifuged at 4000 rpm for 5 min (Hermle Z230A centrifuge, Wehingen, Germany) to remove large aggregates. Drug-free QCT NPs were prepared as described above without the addition of CUR. PEGylated NPs were prepared by adding mPEG-SH (50 mg, 10 mM) to the DMSO solution. DiR-labeled NPs were prepared by mixing QCT (10 mg), DiR (0.1 mg), TEA (9.2 μL), and mPEG-SH (50 mg) in 1 mL DMSO. The composition of the different NP formulations is detailed in Table 1. NPs were lyophilized as needed using a FreeZone 4.5 L Benchtop Freeze Dryer (Labconco Corporation, Kansas City, MO, USA).

Particle size and zeta potential measurements

Particle size and zeta potential of the NPs prepared in this study were measured by dynamic light scattering (DLS) using a Nicomp Nano Z3000 particle size/zeta potential analyzer (Particle Sizing Systems, Santa Barbara, CA, USA). Freshly prepared NPs diluted in ultrapure water were used for the analysis. Each measurement was performed at least three times using different batches of the NPs.

FT-IR and UV-Vis spectroscopy

FT-IR spectra of QCT and QCT NPs were recorded using a Shimadzu IR Affinity-1 spectrometer (Kyoto, Japan), where all samples were prepared as KBr discs (Sigma-Aldrich). UV-Vis spectroscopy was used to determine the presence of free -OH groups using NaOMe and $AlCl_3$/HCl as shift reagents.[23-24] First, the spectra of QCT and QCT NPs (10 μg/mL in methanol) were recorded. Three drops of 1 M NaOMe methanolic solution was then added to each sample and the spectra were immediately recorded. The $AlCl_3$ spectrum was recorded immediately after adding 6 drops of 50 mg/mL $AlCl_3$ methanolic solution to another sample of QCT and QCT NPs.

The $AlCl_3$/HCl spectrum was recorded immediately after adding 3 drops of 5 N HCl to the $AlCl_3$ samples. All analyses were performed using a UV-1800 Shimadzu spectrophotometer (Kyoto, Japan).

Antioxidant activity

DPPH radical scavenging activity of QCT NPs compared to QCT was tested as previously reported.[22] For the assay, 0 – 1000 μg of each material was dissolved in 200 μL ethanol. The solutions were immediately added to 4 mL DPPH (0.1 mM in ethanol) and incubated at RT in the dark for 30 min. The absorbance of the solutions was then measured at 517 nm by UV-Vis (UV-1800 Shimadzu spectrophotometer). Scavenging activity (I) was calculated according to Equation (1):

$$I = [1 - (A_t - A_b)/A_c] \times 100\% \quad (1)$$

where A_t is the absorbance of each test material upon incubation with DPPH, A_b is the background absorbance of each test material without DPPH, and A_c is the absorbance of DPPH alone.

Scanning electron microscopy (SEM) imaging

A drop of NPs suspended in ultrapure water was placed on double-sided carbon tape mounted on an aluminum stub and left to dry overnight prior to imaging using a Versa 3D microscope (FEI, Netherlands) at an accelerating voltage of 2 kV and a working distance of 10 mm.

Drug loading and loading efficiency determination

The amount of CUR loaded into the NPs was determined by diluting 100 μL of the NPs dispersed in water with 900 μL DMSO, followed by measuring the UV absorbance at 430 nm (UV-1800 Shimadzu spectrophotometer). The concentration of CUR was determined based on a standard curve of CUR absorbance vs. concentration in DMSO at 430 nm. Each measurement was repeated at least three times using different batches of the NPs. Drug loading and loading efficiency were calculated according to Equations (2) and (3) as follows:

Drug loading = Actual weight of CUR in NPs / Theoretical weight of QCT NPs (2)

Loading efficiency =

(Actual weight of CUR in NPs / Theoretical weight of CUR in NPs) × 100% (3)

XPS analysis

Successful PEGylation of CUR-loaded and drug-free QCT NPs was verified by XPS. Briefly, gold-coated silicon substrates (Micro to Nano V.O.F., Haarlem, Netherlands) were cleaned by consecutive sonication in deionized distilled water, acetone, and isopropanol for 10 min each, followed by drying under a stream of N_2 and then plasma discharge (HPT-100 Henniker Plasma surface treatment system, Runcorn, UK) at 60% power for 5 min. A drop of each NP dispersion was placed onto the surface of the substrates and left to dry overnight. XPS measurements were carried out using a Thermo Fisher Scientific K-Alpha spectrometer utilizing a 72 W monochromated Al Kα x-ray source (with photon energy of 1,486 eV). The beam was focused to a spot size of 400 microns diameter on the sample surface, defining the analysis area, and three spots were scanned per sample. A dual beam flood gun was used to compensate for sample charging. Survey scans were performed between 0 and 1200 eV electron binding energies.

Elemental composition was obtained from high-resolution spectra of the C 1s, O 1s, and S 2p regions. Charge correction was performed by setting the C 1s peak at 285 eV. Data analysis and peak deconvolution was conducted using CasaXPS.

In vitro release of CUR from CUR-loaded NPs

One milliliter of freshly prepared PEGylated CUR-loaded NPs (NP5; Table 1) was transferred to a dialysis membrane (12 – 14 kD MWCO, Spectra/Por 2, Spectrum Laboratories Inc.) and then immersed in 30 mL PBS containing 0.5% Tween 20 in a tightly closed glass vial. The entire setup was placed in an orbital shaking water bath incubator (GFL 1083, Burgwedel, Germany) operating at 100 rpm and 37 °C. Samples (10 mL) were periodically withdrawn from the release medium and replaced with an equal volume of the buffer. The amount of CUR released at each time point was determined by measuring the fluorescence of the samples at 460/40 nm excitation and 528/20 nm emission using a Biotek FLx800 fluorescence microplate reader (Winooski, VT, USA), based on a standard curve of CUR fluorescence vs. concentration in the same release medium. The results were plotted as cumulative % amount of CUR released vs. time.

Cell culture

The CT26 murine colon carcinoma cell line (ATCC, Manassas, VA, USA) was used throughout this study. Cells were grown as a monolayer in RPMI 1640 medium (Invitrogen, Carlsbad, CA, USA) supplemented with 10% fetal calf serum, 1% L-glutamine, 100 U/mL penicillin, and 100 µg/mL streptomycin (Invitrogen) at 37 °C in 5% CO_2, and passaged twice a week using Trypsin/EDTA (Invitrogen) at 80% confluency.

Cytotoxicity studies

In vitro cytotoxicity of CUR-loaded NPs was evaluated by means of an MTT assay. For the experiment, cells were seeded in 96-well plates at a density of 1×10^4 cells per well (n = 4). After 24 h, media was removed and cells were treated with free CUR, CUR-loaded NPs (NP3 or NP5) at concentrations ranging from 1 – 1,000 μM CUR in complete RPMI 1640 for 72 h. Another set of cells was treated with drug-free PEGylated QCT NPs (C2; 1 – 1,000 μg/mL). At the end of the incubation period, media was removed, replaced with fresh complete RPMI 1640 (100 μL/well) containing 0.5 mg/mL MTT reagent, and cells were incubated for an additional 3 h. Then, the media was carefully removed, 100 μL DMSO was added to each well to dissolve the formazan crystals, and absorbance was read at 570 nm using a microplate reader (FLUOstar Optima, BMG Labtech, Ortenberg, Germany). Cell viability was expressed as % cell survival relative to untreated controls. IC50 was determined by fitting the data into a dose-response curve using Graphpad Prism 6.0e.

Cellular uptake studies

Cellular uptake was evaluated in CT26 cells by confocal laser scanning microscopy (CLSM) and flow cytometry. For confocal microscopy, cells were seeded in 4-well chamber slides (Nunc Lab-Tek, Thermo Scientific, Rochester, NY, USA) at a density of 1×10^5 cells per well and incubated in complete RPMI 1640 for 24 h. Cells were then treated with 500 μL of CUR or CUR-loaded QCT NPs (NP3 and NP5) at concentrations equivalent to 20 μM CUR in complete RPMI 1640 for 24 h. At the end of the incubation period, cells were washed three times with PBS and then fixed in 4% paraformaldehyde for 10 min at RT. The fixed cells were washed twice with PBS, mounted with ProLong™ Diamond antifade mountant with DAPI (Invitrogen),

and covered with glass cover slips. Uptake was visualized using a Zeiss LSM 780 microscope (Carl Zeiss GmbH, Gena, Germany). The 405 and 488 nm lines of a diode laser were used for the excitation of DAPI and FITC, respectively. Emission was filtered between 441 – 495 nm and 495 – 590 nm for DAPI and FITC, respectively. Images were captured using a Plan-Apochromat 20×/0.8 M27 objective, and were acquired at a box size of 1904 × 1904 pixels, a scan speed of 4 fps (6.78 μs per pixel), and an average line scan of 1. All obtained images were processed using Zen software (Carl Zeiss) and ImageJ version 1.51m9 (NIH, Bethesda, MD, USA).

For flow cytometry analysis, cells were seeded in 24-well plates at a density of 1×10^5 cells per well, allowed to attach overnight, and then treated with 500 μL of CUR or CUR-loaded QCT NPs (NP3 and NP5) at concentrations equivalent to 20 μM CUR in complete RPMI 1640 for 24 h. After treatment, the cells were washed twice with PBS, trypsinized, resuspended, and centrifuged at 1500 rpm for 5 min. Cell pellets were resuspended in 250 μL of PBS. Cellular internalization of CUR or its NP formulations was quantified by detecting CUR's fluorescence using the FL2 channel detector on a BD FACSCalibur flow cytometer (BD Biosciences, San Jose, CA, USA) from at least 10,000 gated cells per sample. The measurements were performed in triplicate and presented as mean ± SD.

Organ biodistribution studies by in vivo imaging

All animal experiments were performed in compliance with the UK Home Office (1989) Code of Practice for the housing and care of Animals used in Scientific Procedures. Four to six weeks-old female Balb/c mice (weighing ~20 g) (Envigo) were inoculated subcutaneously with CT26 cells (1×10^6 cells in 0.1 mL PBS) at the lower right flank. Mice (n = 3) were intravenously injected with DiR-labeled PEGylated QCT NPs in PBS at a dose of 18.75 μg/kg DiR and imaged

at 1, 4, and 24 h post-injection using an IVIS Lumina Series III In Vivo Imaging System (Caliper Life Sciences, Perkin Elmer, USA). Untreated animals were also included as controls. Animals were anesthetized with 1.5% isoflurane/98.5% oxygen to maintain sedation during the imaging procedure. Ex vivo imaging was carried out immediately afterward by imaging excised major organs (heart, lung, liver, spleen, intestine, stomach, and kidney) as well as tumors. Fluorescence images were obtained using the DiR filter (680, 700, 720, 740, and 760/790 nm for excitation/emission wavelengths) with an exposure time of 1 s. All images were captured using a sequential acquisition spectra unmixing mode and were obtained using binning factor of 4, f number of 2, and field of view of D-12.5 cm. The collected fluorescence emission signals were stored in efficiency units.

Tumor uptake of systemically administered NPs by flow cytometry

For the quantification of CUR-loaded NP uptake in tumor tissue, female Balb/c mice inoculated with CT26 tumors (n = 3) were injected via tail vein with 200 μL of NP5 (6 mg CUR/ kg) dispersed in PBS. At 30 h post-injection, animals were sacrificed and tumors were excised. Tumors were placed in a 6-well plate containing 2 mL serum-free RPMI 1640 and cut into small pieces using a scalpel. Two milliliters of serum-free medium was added to each well and the chopped pieces were transferred to universal test tubes. Digestion enzymes (collagenase type IV and DNase I) were added to each tube at a final concentration of 2 mg/mL and 150 μg/mL for collagenase type IV and DNase I, respectively. Tumor pieces were then incubated for 45 min at 37 °C in a shaking water bath, vortexing every 15 min for 30 sec. After, 10 mL of 1% FBS in PBS was added to each tube, and the digested tissues were filtered using a 70 μm cell strainer in order to obtain uniform cell suspensions. The filtered suspensions were each centrifuged at 500

× g for 5 min at 4 °C, the supernatants were discarded, and the pellets were resuspended in 10 mL PBS. Samples were centrifuged again at 500 × g for 5 min at 4 °C, the supernatants were discarded and cell pellets were resuspended in 1X ACK buffer for 5 min, followed by adding 25 mL PBS to each sample. Cell suspensions were centrifuged again at 500 × g for 5 min at 4 °C, and the pellets were resuspended in 200 µL PBS for flow cytometry analysis as described above. Tumor homogenates of untreated animals were used as control.

Statistical analysis

Statistical analysis was performed in Graphpad Prism 6.0e using a 1-way analysis of variance (ANOVA) followed by Tukey's multiple comparisons test, where $p < 0.05$ was considered statistically significant.

Acknowledgments

S.S. acknowledges funding from Al-Zaytoonah University of Jordan (Grant no. 15/28/2017-2018), PhosAgro/UNESCO/IUPAC Partnership in Green Chemistry for Life (Contract no. 4500378258), TWAS-COMSTECH (Grant no. 17-134 RG/MSN/AF/AC_C-FR3240300066), and the Academy of Medical Sciences (2018 Daniel Turnberg Travel Fellowship). XPS data collection was performed at the EPSRC National Facility for XPS ('HarwellXPS') under contract No. PR16195. The authors would like to thank Rula Baqain and Aya Abusheikha from the Cell Therapy Center, Amman, Jordan for assistance with SEM imaging and confocal microscopy.

Supporting Information Available: FT-IR, UV-Vis, and deconvoluted high-resolution XPS spectra, and results from DPPH and cell viability assays. This material is available free of charge *via* the Internet at http://pubs.acs.org.

Tables and Figures

Table 1. Summary of the different NPs synthesized in this study.

NP	QCT: CUR (mol/mol)	QCT (mg)	CUR (mg)
C1	-	10.0	-
C2[a]	-	10.0	-
NP1	1:1	10.0	12.2
NP2	1:0.5	10.0	6.1
NP3	1:0.25	10.0	3.0
NP4	1:0.1	10.0	1.2
NP5[a]	1:0.25	10.0	3.0

[a]PEGylated NP

Table 2. Characterization of the NPs synthesized in this study.

NP	Particle size (nm)	PDI[b]	Zeta potential (mV)	Loading (μg CUR/mg NP)	Loading efficiency (%)
C1	33.4 ± 5.2	0.40 ± 0.01	-16.3 ± 1.1	-	-
C2[a]	165.6 ± 34.8	0.37 ± 0.09	-11.3 ± 1.2	-	-
NP1	76.4 ± 6.1	0.38 ± 0.03	-17.6 ± 1.6	5.8 ± 2.3	4.7 ± 1.9
NP2	69.3 ± 24.3	0.46 ± 0.05	-16.7 ± 1.2	6.0 ± 2.7	9.9 ± 4.8
NP3	139.9 ± 2.4	0.05 ± 0.03	-21.7 ± 0.8	27.7 ± 1.8	91.0 ± 6.0
NP4	96.6 ± 17.7	0.22 ± 0.02	-16.9 ± 0.8	6.3 ± 1.5	51.2 ± 13.5
NP5[a]	90.2 ± 1.8	0.13 ± 0.01	-11.6 ± 1.0	15.5 ± 9.8	51.1 ± 6.5

[a]PEGylated NP; [b]Polydispersity index

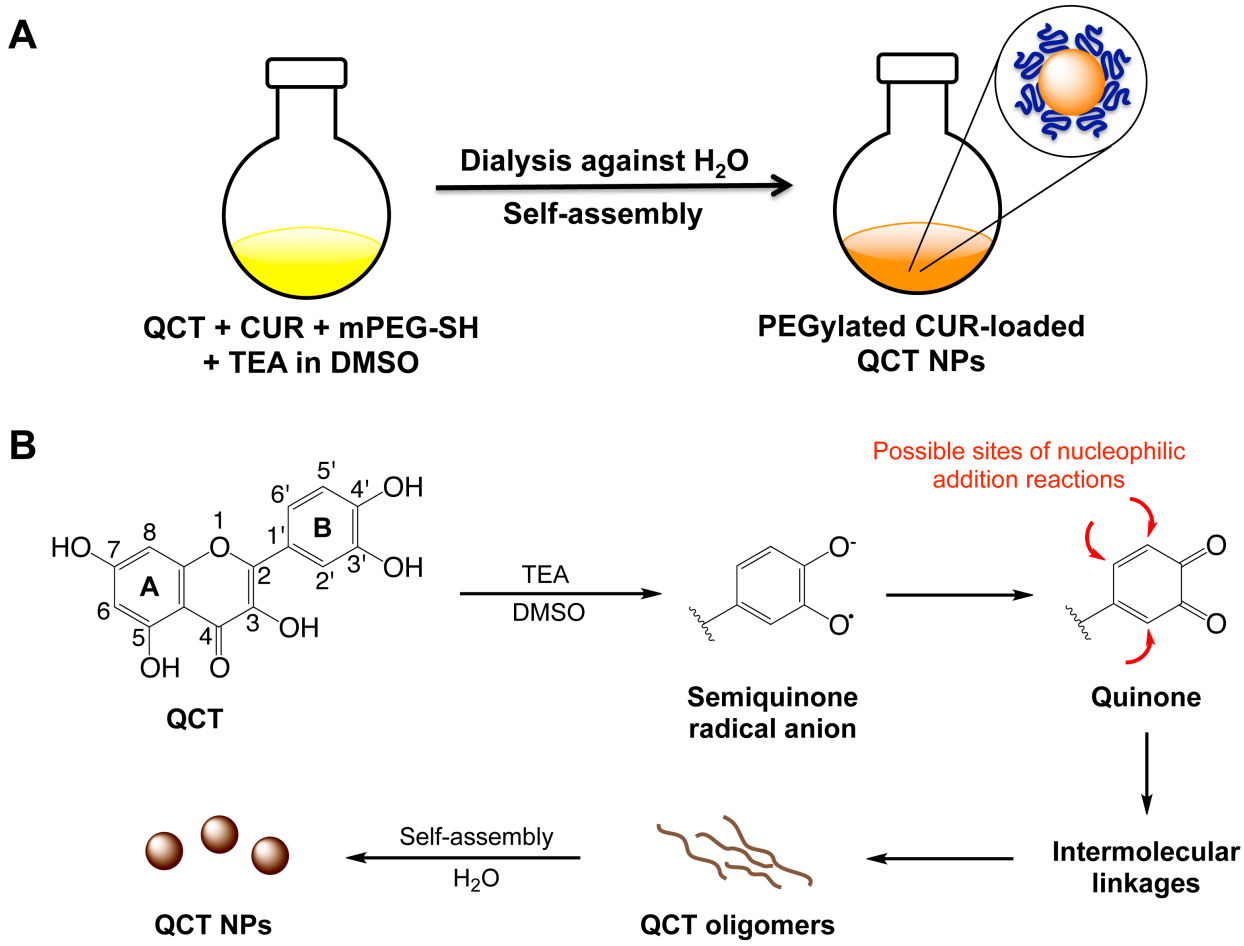

Figure 1. (A) One-pot synthesis of PEGylated CUR-loaded QCT NPs. (B) Proposed NP formation mechanism by base-catalyzed oxidative polymerization of QCT and subsequent self-assembly into NPs.

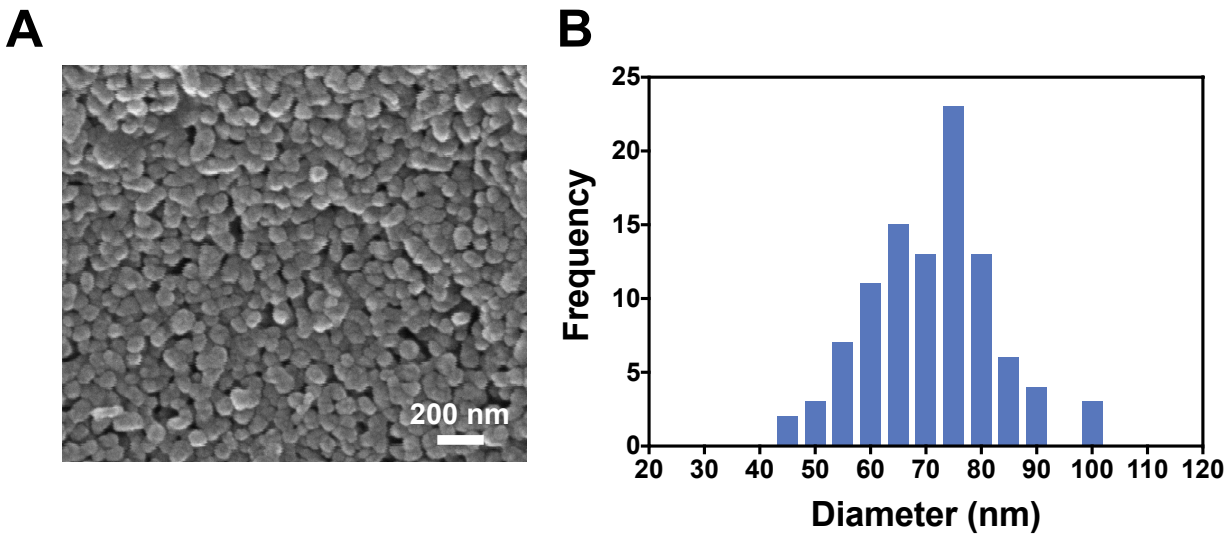

Figure 2. (A) SEM image of PEGylated CUR-loaded NPs (NP5) showing their spherical morphology. (B) Frequency distribution histogram of NP diameter obtained by analyzing 100 NPs from the SEM image using ImageJ. The mean diameter was calculated to be 71.0 ± 11.3 nm.

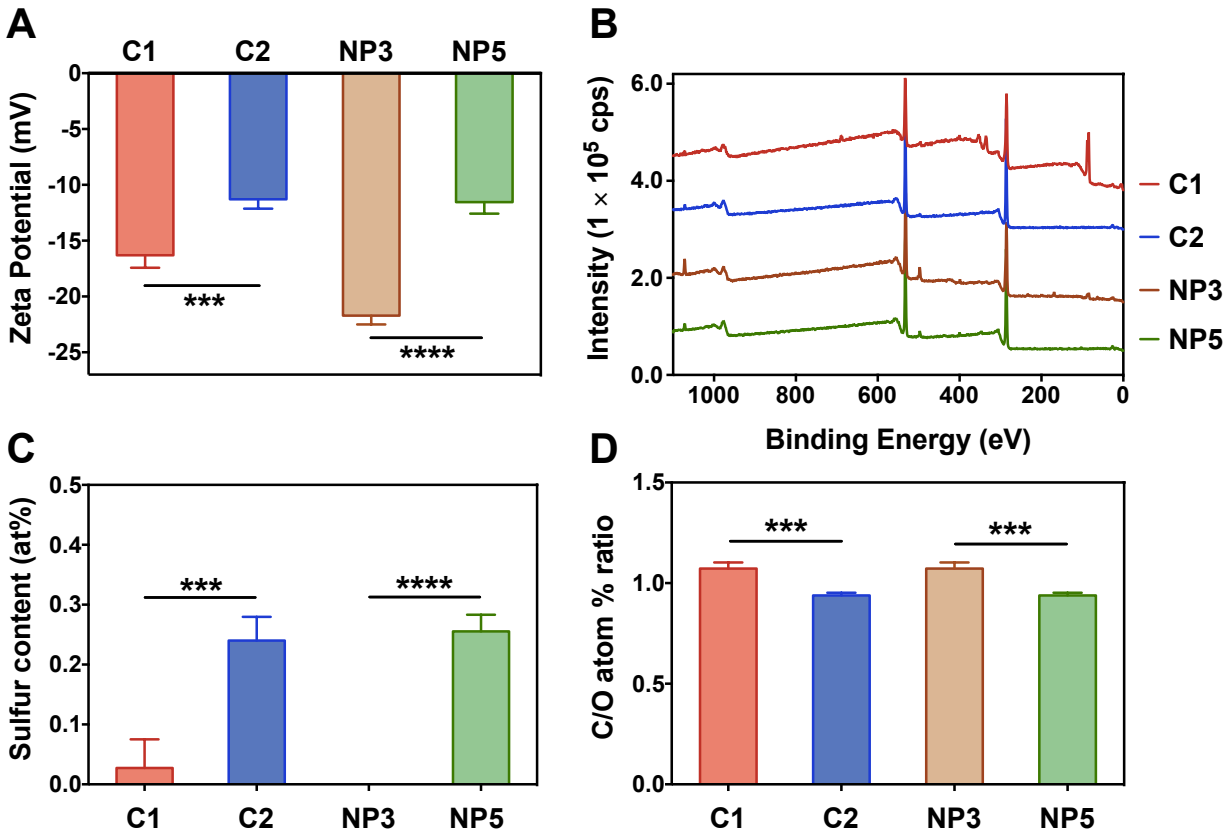

Figure 3. Confirmation of NP PEGylation by DLS and XPS. (A) Zeta potential of QCT NPs (C1), PEGylated QCT NPs (C2), CUR-loaded QCT NPs (NP3) and PEGylated CUR-loaded QCT NPs (NP5). A significant reduction in zeta potential was observed after PEGylation, which verifies successful surface modification of C2 and NP5 NPs with mPEG-SH. (B) Representative XPS survey spectra of C1, C2, NP3, and NP5. (C) Sulfur content of QCT NPs measured by XPS. A significant increase in S 2p signals was observed after PEGylation, which further confirms surface modification of C2 and NP5 NPs with mPEG-SH. (D) A significant reduction in C/O atom % ratio signifies an increase in C-O-C components on the surface of C2 and NP5 consistent with PEGylation. *** $p < 0.001$; **** $p < 0.0001$.

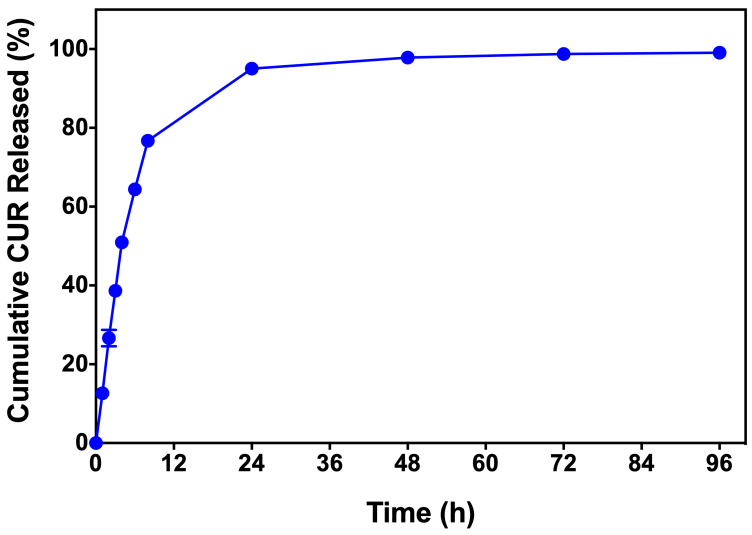

Figure 4. Cumulative release of CUR from PEGylated CUR-loaded QCT NPs (NP5; n = 3) in PBS pH 7.4 showing sustained release over 4 days.

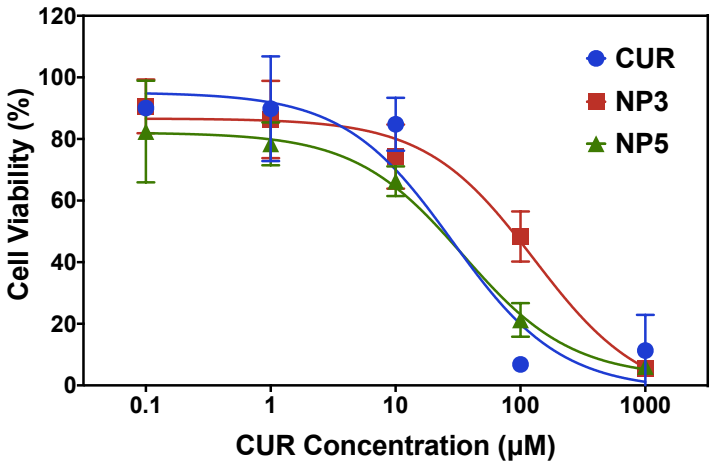

Figure 5. Cell viability of CT26 cells after 72 h incubation with 0 – 1000 μM CUR, CUR-loaded QCT NPs (NP3), or PEGylated CUR-loaded QCT NPs (NP5) (n = 4). Free CUR and NP5 exhibited comparable potency with an IC50 of 28.5 and 34.7 μM, respectively, whereas NP3 showed lower potency with an IC50 of 128.3 μM.

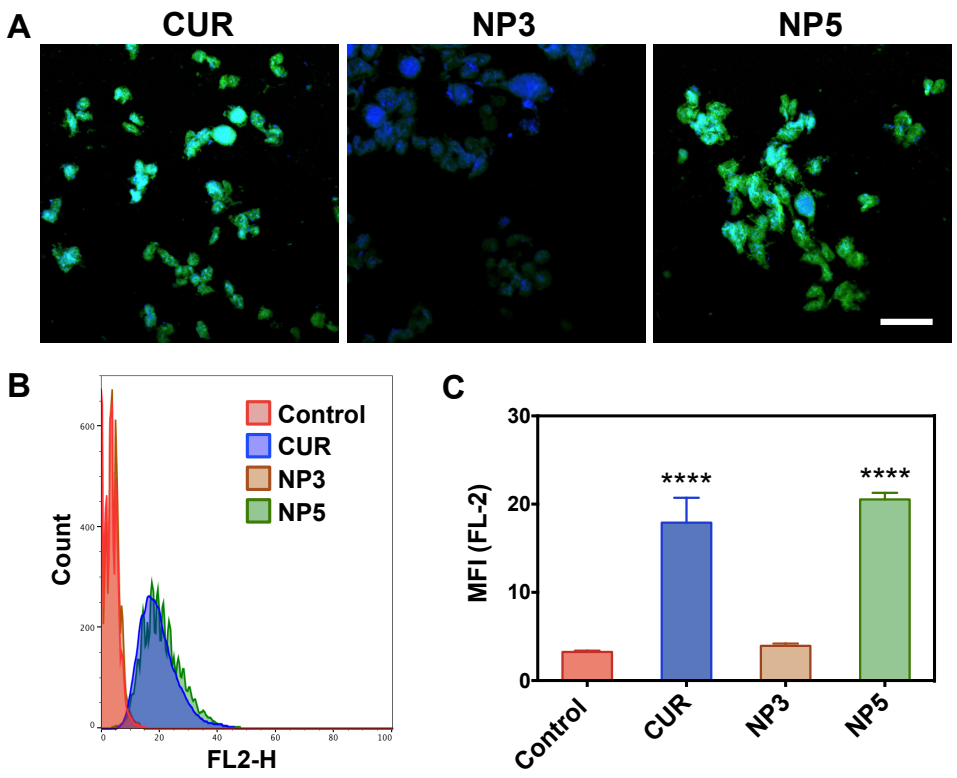

Figure 6. Cellular uptake of CUR and its NP formulations in CT26 cells. (A) Confocal microscopy images of CT26 cells treated with 20 μM free CUR, nonPEGylated CUR-loaded NPs (NP3), or PEGylated CUR-loaded NPs (NP5) for 24 h. Uptake of NP5 was comparable to free CUR as indicated by the strong intracellular green fluorescence signals, while NP3 showed much weaker fluorescence signals signifying reduced cellular uptake. Blue: cell nuclei stained by DAPI; green: CUR; scale bar = 20 μm. (B) Representative flow cytometry histograms of CT26 cells treated with CUR, NP3, or NP5 for 24 h (n = 3). (C) Mean fluorescence intensities (MFI) of the FL-2 channel showing significantly higher cell-associated fluorescence for CUR- and NP5-treated cells compared to control and NP3, consistent with confocal microscopy observations. **** $p < 0.0001$.

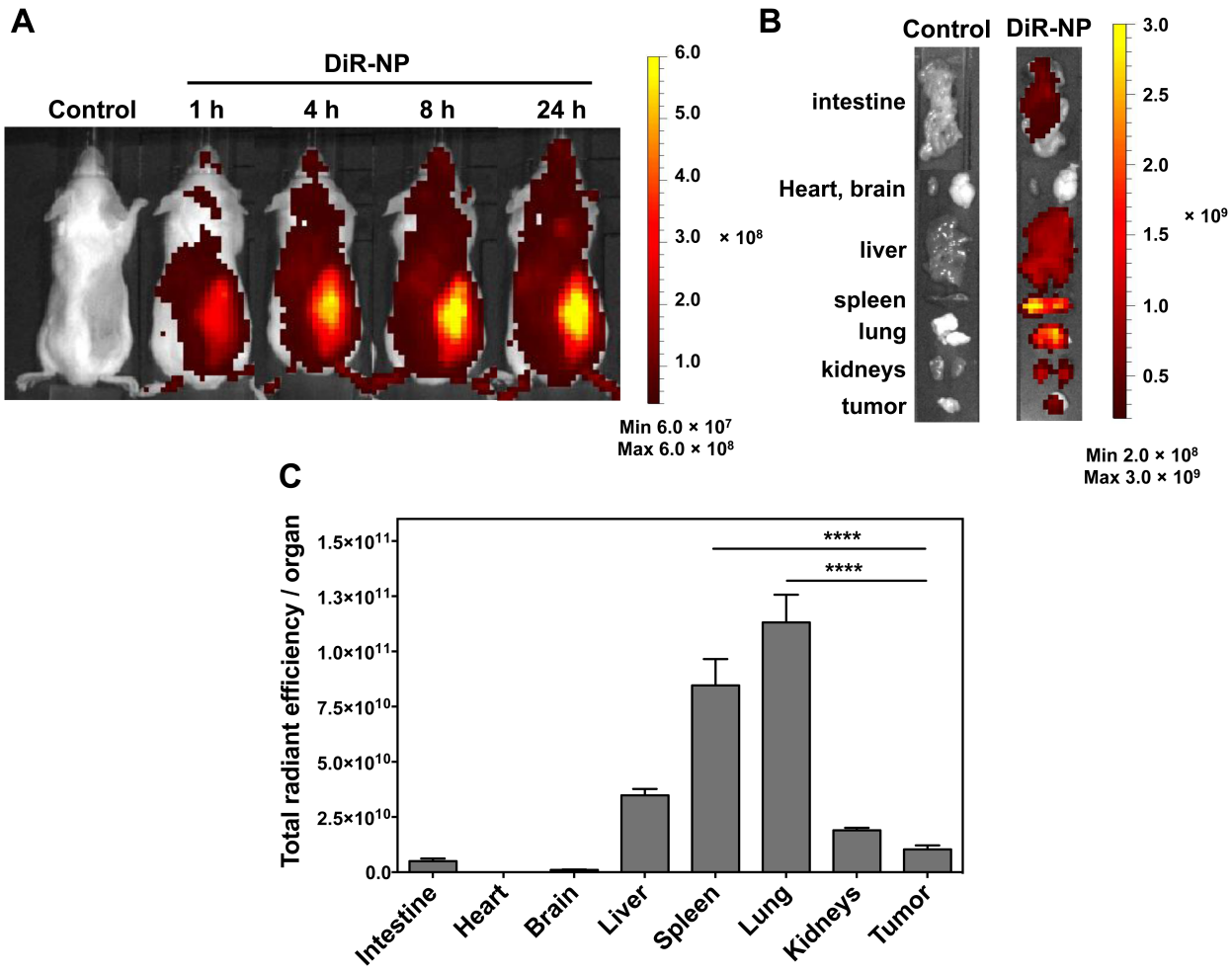

Figure 7. In vivo and ex vivo organ biodistribution of IV-administered DiR-labeled PEGylated QCT NPs in CT26 tumor-bearing Balb/c mice (n = 3). (A) Representative whole body in vivo images (dorsal view) of DiR-NP-treated animals compared to PBS-treated control obtained at 1, 4, 8, and 24 h post-injection showing a steady increase in tumor accumulation of the NPs. (B) Representative ex vivo images of excised organs at 24 h post-injection. (C) Quantified fluorescence signals of excised organs expressed as total radiant efficiency/g organ after subtracting background fluorescence. Although in vivo images showed significant accumulation of the NPs around the tumor, fluorescence intensities of excised lung and spleen were significantly higher than those of the tumors, which suggests that the NPs may still be present in the tumor vasculature at 24 h. **** $p < 0.0001$.

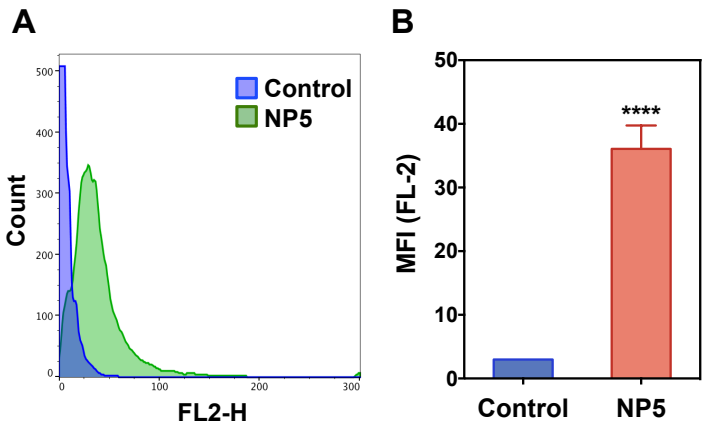

Figure 8. Tumor uptake of IV-administered PEGylated CUR-loaded NPs (NP5) at 6 mg/kg CUR in CT26 tumor-bearing Balb/c mice (n = 3). Tumors were excised 30 h post-injection and tissue homogenates were analyzed by flow cytometry. (A) Representative flow cytometry histograms and (B) corresponding MFI of tumor homogenates from untreated and NP5-treated animals showing significant tumor accumulation of CUR. **** $p < 0.0001$.

References

1. WHO Cancer Fact Sheet. http://www.who.int/mediacentre/factsheets/fs297/en/ (accessed Dec 29).

2. Popovic, Z.; Liu, W. H.; Chauhan, V. P.; Lee, J.; Wong, C.; Greytak, A. B.; Insin, N.; Nocera, D. G.; Fukumura, D.; Jain, R. K.; Bawendi, M. G., A Nanoparticle size series for in vivo fluorescence imaging. *Angew. Chem.-Int. Edit.* **2010,** *49* (46), 8649-8652.

3. Ulbrich, K.; Hola, K.; Subr, V.; Bakandritsos, A.; Tucek, J.; Zboril, R., Targeted drug delivery with polymers and magnetic nanoparticles: Covalent and noncovalent approaches, release control, and clinical studies. *Chemical Rev.* **2016,** *116* (9), 5338-5431.

4. Sunoqrot, S.; Hamed, R.; Abdel-Halim, H.; Tarawneh, O., Synergistic interplay of medicinal chemistry and formulation strategies in nanotechnology – From drug discovery to nanocarrier design and development. *Curr. Topic. Med. Chem.* **2017,** *17* (13), 1451-1468.

5. Nicolas, J.; Mura, S.; Brambilla, D.; Mackiewicz, N.; Couvreur, P., Design, functionalization strategies and biomedical applications of targeted biodegradable/biocompatible polymer-based nanocarriers for drug delivery. *Chem. Soc. Rev.* **2013,** *42* (3), 1147-1235.

6. Torchilin, V. P., Multifunctional, stimuli-sensitive nanoparticulate systems for drug delivery. *Nat. Rev. Drug Discovery* **2014,** *13* (11), 813-827.

7. El-Gogary, R. I.; Rubio, N.; Wang, J. T.-W.; Al-Jamal, W. T.; Bourgognon, M.; Kafa, H.; Naeem, M.; Klippstein, R.; Abbate, V.; Leroux, F., Polyethylene glycol conjugated polymeric nanocapsules for targeted delivery of quercetin to folate-expressing cancer cells in vitro and in vivo. *ACS Nano* **2014,** *8* (2), 1384-1401.

8. Quadir, M. A.; Morton, S. W.; Mensah, L. B.; Shopsowitz, K.; Dobbelaar, J.; Effenberger, N.; Hammond, P. T., Ligand-decorated click polypeptide derived nanoparticles for targeted drug delivery applications. *Nanomedicine* **2017,** *13* (5), 1797-1808.

9. Zhou, Z.; Badkas, A.; Stevenson, M.; Lee, J.-Y.; Leung, Y.-K., Herceptin conjugated PLGA-PHis-PEG pH sensitive nanoparticles for targeted and controlled drug delivery. *Int. J. Pharm.* **2015,** *487* (1), 81-90.

10. Banerjee, A.; Qi, J.; Gogoi, R.; Wong, J.; Mitragotri, S., Role of nanoparticle size, shape and surface chemistry in oral drug delivery. *J. Controlled Release* **2016,** *238*, 176-185.

11. Lee, H. A.; Ma, Y.; Zhou, F.; Hong, S.; Lee, H., Material-independent surface chemistry beyond polydopamine coating. *Acc. Chem. Res.* **2019,** *52* (3), 704-713.

12. Lee, H.; Dellatore, S. M.; Miller, W. M.; Messersmith, P. B., Mussel-inspired surface chemistry for multifunctional coatings. *Science* **2007,** *318* (5849), 426-430.

13. Lee, H.; Rho, J.; Messersmith, P. B., Facile conjugation of biomolecules onto surfaces via mussel adhesive protein inspired coatings. *Adv. Mater.* **2009,** *21* (4), 431-434.

14. Li, J.; Wu, S. X.; Wu, C. C.; Qiu, L. P.; Zhu, G. Z.; Cui, C.; Liu, Y.; Hou, W. J.; Wang, Y. Y.; Zhang, L. Q.; Teng, I. T.; Yang, H. H.; Tan, W. H., Versatile surface engineering of porous nanomaterials with bioinspired polyphenol coatings for targeted and controlled drug delivery. *Nanoscale* **2016,** *8* (16), 8600-8606.

15. Abouelmagd, S. A.; Meng, F. F.; Kim, B. K.; Hyun, H.; Yeo, Y., Tannic acid-mediated surface functionalization of polymeric nanoparticles. *ACS Biomater. Sci. Eng.* **2016,** *2* (12), 2294-2303.

16. Liu, Y.; Ai, K.; Liu, J.; Deng, M.; He, Y.; Lu, L., Dopamine-melanin colloidal nanospheres: An efficient near-infrared photothermal therapeutic agent for in vivo cancer therapy. *Adv. Mater.* **2013,** *25* (9), 1353-1359.

17. Ju, K.-Y.; Lee, Y.; Lee, S.; Park, S. B.; Lee, J.-K., Bioinspired polymerization of dopamine to generate melanin-like nanoparticles having an excellent free-radical-scavenging property. *Biomacromolecules* **2011,** *12* (3), 625-632.

18. Amin, D. R.; Sugnaux, C.; Lau, K. H. A.; Messersmith, P. B., Size control and fluorescence labeling of polydopamine melanin-mimetic nanoparticles for intracellular imaging. *Biomimetics* **2017,** *2* (3), 17.

19. Chen, Z.; Wang, C.; Chen, J.; Li, X., Biocompatible, functional spheres based on oxidative coupling assembly of green tea polyphenols. *J. Am. Chem. Soc.* **2013,** *135* (11), 4179-4182.

20. Markova, Z.; Novak, P.; Kaslik, J.; Plachtova, P.; Brazdova, M.; Jancula, D.; Siskova, K. M.; Machala, L.; Marsalek, B.; Zboril, R., Iron (II, III)–polyphenol complex nanoparticles derived from green tea with remarkable ecotoxicological impact. *ACS Sustainable Chem. Eng.* **2014,** *2* (7), 1674-1680.

21. Xiang, S.; Yang, P.; Guo, H.; Zhang, S.; Zhang, X.; Zhu, F.; Li, Y., Green tea makes polyphenol nanoparticles with radical-scavenging activities. *Macromol. Rapid Commun.* **2017,** *38* (23), 1700446.

22. Sunoqrot, S.; Al-Shalabi, E.; Messersmith, P. B., Facile synthesis and surface modification of bioinspired nanoparticles from quercetin for drug delivery. *Biomater. Sci.* **2018,** *6* (10), 2656-2666.

23. Markham, K. R.; Mabry, T. J., A procedure for the ultraviolet spectral detection of ortho-dihydroxyl groups in flavonoids. *Phytochemistry* **1968,** *7* (7), 1197-1200.

24. Suh, H. J.; Lee, J. M.; Cho, J. S.; Kim, Y. S.; Chung, S. H., Radical scavenging compounds in onion skin. *Food Res. Int.* **1999,** *32* (10), 659-664.

25. Cornard, J. P.; Boudet, A. C.; Merlin, J. C., Complexes of Al(III) with 3′4′-dihydroxy-flavone: Characterization, theoretical and spectroscopic study. *Spectrochim. Acta, Part A* **2001,** *57* (3), 591-602.

26. Amin, D. R.; Higginson, C. J.; Korpusik, A. B.; Gonthier, A. R.; Messersmith, P. B., Untemplated resveratrol-mediated polydopamine nanocapsule formation. *ACS Appl. Mater. Interfaces* **2018,** *10* (40), 34792-34801.

27. Klippstein, R.; Wang, J. T. W.; El-Gogary, R. I.; Bai, J.; Mustafa, F.; Rubio, N.; Bansal, S.; Al-Jamal, W. T.; Al-Jamal, K. T., Passively targeted curcumin-loaded PEGylated PLGA nanocapsules for colon cancer therapy in vivo. *Small* **2015,** *11* (36), 4704-4722.

28. Ye, Q.; Zhou, F.; Liu, W. M., Bioinspired catecholic chemistry for surface modification. *Chem. Soc. Rev.* **2011,** *40* (7), 4244-4258.

29. Ho, C.-C.; Ding, S.-J., The pH-controlled nanoparticles size of polydopamine for anti-cancer drug delivery. *J. Mater. Sci.: Mater. Med.* **2013,** *24* (10), 2381-2390.

30. Yu, X.; Tang, X.; He, J.; Yi, X.; Xu, G.; Tian, L.; Zhou, R.; Zhang, C.; Yang, K., Polydopamine nanoparticle as a multifunctional nanocarrier for combined radiophotodynamic therapy of cancer. *Part. Part. Syst. Charact.* **2017,** *34* (2), 1600296.

31. Zhang, X.; Wang, S.; Xu, L.; Feng, L.; Ji, Y.; Tao, L.; Li, S.; Wei, Y., Biocompatible polydopamine fluorescent organic nanoparticles: Facile preparation and cell imaging. *Nanoscale* **2012,** *4* (18), 5581-5584.

32. El Yakhlifi, S.; Ihiawakrim, D.; Ersen, O.; Ball, V., Enzymatically active polydopamine @ alkaline phosphatase nanoparticles produced by NaIO4 oxidation of dopamine. *Biomimetics* **2018,** *3* (4), 36-48.

33. Saowalak, K.; Titipun, T.; Somchai, T.; Chalermchai, P., Iron(III)-tannic molecular nanoparticles enhance autophagy effect and T1 MRI contrast in liver cell lines. *Sci. Rep.* **2018,** *8* (1), 6647.

34. You, I.; Jeon, H.; Lee, K.; Do, M.; Seo, Y. C.; Lee, H. A.; Lee, H., Polydopamine coating in organic solvent for material-independent immobilization of water-insoluble molecules and avoidance of substrate hydrolysis. *J. Ind. Eng. Chem.* **2017,** *46*, 379-385.